RSC Advances

PAPER

View Article Online
View Journal | View Issue

Cite this: *RSC Adv.*, 2025, **15**, 37288

Study of the electronic, magnetic, and thermoelectric aspects of spinel chalcogenides $SrCe_2Z_4$ (Z = Te, Se, S) for spintronic and energy applications

Muhammad Furqan,[a] Ghulam M. Mustafa, *[a] Hanof Dawas Alkhaldi,[b] Fawziah Alhajri,[c] G. I. Ameereh,[c] Murefah mana Al-Anazy, *[d] Ali El-Rayyes[e] and Q. Mahmood*[fg]

Spinel chalcogenides are promising candidates for the advancement of spintronic and thermoelectric devices. Therefore, this article presents the structural, electronic, and magnetic characteristics of $SrCe_2Z_4$ (Z = S, Se, Te) spinels employing WIEN2k in the context of density functional theory. The expansion of the unit cell is witnessed with the incorporation of larger anions and lattice parameters, including 12.01 Å for $SrCe_2S_4$, 12.52 Å for $SrCe_2Se_4$, and 13.42 Å for $SrCe_2Te_4$. The maximum release of energy in the FM states (rather than AFM states) and the negative enthalpy of formation (−2.20 eV, −2.05 eV, and −1.94 eV) confirm their dominant ferromagnetic nature and the thermodynamic stability of the system. The spin-polarized band structure exhibits the ferromagnetic semiconducting nature of $SrCe_2S_4$ and $SrCe_2Te_4$, as well as the half-metallic ferromagnetic behavior of $SrCe_2Se_4$. The analysis of the total density of states also endorses the exact nature predicted during the band structure investigation. The magnetic properties are explored by calculating the direct exchange energy Δ_x(f), indirect exchange energy Δ_x(pf), along with the exchange constants $N_o\alpha$ and $N_o\beta$ to analyze the magnetic behavior. The significant hybridization of chalcogenide's 2p states and the f states from the Ce atom located at the Fermi level results in the total magnetic moments. All these compositions reveal that the Curie temperature is near or above room temperature. The thermoelectric characteristics of the spinels are examined utilizing the BoltzTrap code to inspect the parameters including power factors and the figure of merit as a function of temperature. The *ZT* value of 0.90 for $SrCe_2Te_4$ indicates its higher thermoelectric efficiency and potential for future thermoelectric devices.

Received 13th May 2025
Accepted 16th September 2025

DOI: 10.1039/d5ra03092g

rsc.li/rsc-advances

1. Introduction

The high energy consumption, low processing speed, and large size of traditional electronic devices make them outdated, emphasizing the need for novel nanoscale chips that are more effective, faster, and more appropriate for cutting-edge technologies.[1] Nowadays, spintronics is one of the emerging fields that uses both the spin and charge of electrons, offering significant potential for next-generation electronic devices.[2] Electrons exist in two spin channels, *i.e.*, spin-up (S↑) and spin-down (S↓).[3] Understanding spintronics is essential to harness the full potential of electron spin to revolutionize the electronics industry, as it enables a wide range of innovative applications in data processing and storage.[2] The identification of giant magnetoresistance (GMR) in 1988 illustrated that under an applied magnetic field, the resistance of a thin magnetic layer significantly changes and can improve the performance of data storage devices. This internal response of electron spin has led to the development of memory devices that offer both rapid access and non-volatility.[4] High spin-polarization is a key to improving the quality, faster data processing, and data storage aptitude of spintronics devices.[5,6] Ferromagnetic (FM) semiconductor materials have the highest spin polarization because of the different semiconducting and insulation properties in the spin majority (S↑) and spin minority (S↓) orientations.[7] For

[a]*Department of Physics, Division of Science and Technology, University of Education, Lahore, Punjab 54770, Pakistan. E-mail: dr.ghulam.muhammad@ue.edu.pk*

[b]*Department of Science and Technology, University College at Nairiyah, University of Hafr Al Batin (UHB), Nairiyah 31981, Saudi Arabia*

[c]*Department of Physics, College of Science & Humanities- Jubail, Imam Abdulrahman Bin Faisal University, Saudi Arabia*

[d]*Department of Chemistry, College of Sciences, Princess Nourah bint Abdulrahman University (PNU), P. O. Box 84428, Riyadh 11671, Saudi Arabia*

[e]*Center for Scientific Research and Entrepreneurship, Northern Border University, 73213, Arar, Saudi Arabia*

[f]*Basic and Applied Scientific Research Center, Imam Abdulrahman Bin Faisal University, P. O. Box 1982, Dammam, 31441, Saudi Arabia*

[g]*Department of Physics, College of Science, Imam Abdulrahman Bin Faisal University, P. O. Box 1982, Dammam, 31441, Saudi Arabia*

potential spintronic devices, the Curie temperature (T_c) must be higher than RT.[8,9] GMR applications mostly involve spin filtering,[10] including spin valves and magnetic field sensors used to form hard disks.[11] Double perovskites, Heusler alloys, and spinels have potential applications in spintronics, but the FM spinels, which have anions from chalcogens, have gained special interest for the newly discovered spintronic applications.[12]

In spintronics, spinel chalcogenides are recognized for their unique structural, electrical, magnetic, and transport characteristics. The empirical formula of spinel is AB_2X_4, in which A and B are cations, and X represents the anions Se, S, Te, and O.[13] The cubic closed-packed arrangements of anions generate the octahedral and tetrahedral sites, which are filled by the cations.[14] In the crystal structure of spinels, the A^{II} resides in 1/8th of the tetrahedral void, and the B^{III} resides in 1/2nd of the octahedral voids.[15] To check whether the spinel structure is normal or inverse, we follow the specific rule that cations are transitional or non-transitional metals.[16] Spinel chalcogenides have exceptional magnetic characteristics, including high magnetoresistance, which changes the electrical resistance in response to applied magnetic fields, making them suitable for magnetic sensing, data storage, and magnetic field modulation applications. In addition, the attractive thermoelectric (TE) properties enhance their utility for energy conversion and processing.[2] Spinels have high thermal and chemical stability.[17] In light of existing literature, it has been observed that no research has been done on spinel composition $SrCe_2Z_4$, which has a wide spectrum of tunable properties, making it promising for advanced applications.[18]

The previous studies reveal that spinels with rare earth metals are considered emerging breakthroughs for spintronics devices.[19] Researchers are particularly interested in spinels having rare earth metals because of their intense spin polarization, which leads to higher magnetoresistance.[20] High magnetoresistance is primarily used in spintronic devices like spin valves, biosensors, magnetic field sensors, and other electronic devices. Hassan *et al.* (2024) reported on the presence of half-metallic ferromagnetism (HMF) with complete spin polarization in Heusler alloys, before moving on to other materials like chalcogenides and spinels.[21] Similarly, Alburaih *et al.* (2024) found that RE-based $MgSm_2Y_4$ (Y = S, Se) spinels exhibited HM ferromagnetism, high SP, and promising TE characteristics, with $MgSm_2S_4$ showing the highest value of *ZT*.[22] Manjunatha *et al.* (2020) investigated the magnetic and electronic characteristics of $Co_{1-x}Sc_xCr_2O_4$ (x = 0.0 and 0.05) nanoparticles by DFT and experimental methods. To better understand the magnetic behavior, field-dependent magnetization and temperature-dependent susceptibility were measured in two magnetic transitions, paramagnetic, collinear ferrimagnetic, and non-collinear spiral states.[23] Maqsood *et al.* (2024) investigated Cd-based spinels $CdSm_2(S/Se)_4$ chalcogenide, and found them suitable for spintronic applications due to their promising magnetic and electrical properties. The total magnetic moment was 10.0 μ_B for both compositions.[24] Noor *et al.* (2024) carried out DFT-based research to inspect the mechanical, electronic, and magnetic properties of $HgSm_2S_4$ and $HgSm_2Se_4$ chalcogenides for spintronic applications. Both compounds exhibited a total magnetic moment of 10.0 μ_B.[25] Kattan *et al.* (2024) investigated the HMF and transport properties of $MgCo_2(S/Se)_4$ chalcogenides for energy harvesting and spintronic implementations. Their study confirmed the half-metallic nature and robust ferromagnetic behavior of these materials, highlighting their potential for high-performance thermoelectric and spintronic devices.[26] In another study, Albalawi *et al.* (2023) inspected $MgEr_2(S/Se)_4$ spinels, revealing stable ferromagnetism, full SP, and showing potential in TE characteristics for energy harvesting.[27] The $SrCe_2Z_4$ spinels, especially $SrCe_2Te_4$, show exceptional thermoelectric efficiency and magnetic nature, positioning them as superior candidates for future thermoelectric and spintronic devices. Khushi *et al.* (2023) performed first-principles simulations on $CdHo_2Y_4$ (Y = S, Se) spinels, demonstrating their ferromagnetic behavior and suitability for energy storage.[28]

Ramzan *et al.* (2022) confirmed HMF and favorable transport characteristics in MgV_2S/Se_4 chalcogenides, indicating their promise in thermoelectric and spintronic applications.[29] Bilal *et al.* (2022) explored the half-metallic ferromagnetism of spinel $MgFe_2Z_4$ (Z = S, Se) chalcogenides for spintronic implementations. Their results verified these material's half-metallic behavior and robust ferromagnetic ordering, highlighting their suitability for advanced spintronic device applications.[30] Alburaih (2021) examined the RE-doped spinels $CdEr_2X_4$ (X = S, Se), reporting strong ferromagnetism and efficient electronic transport for spintronic and energy harvesting applications. The study found that both materials exhibit a total magnetic moment of 5.0 μ_B.[31] Based on the available data, no theoretical analysis has been carried out on the transport and ferromagnetism features of $SrCe_2Z_4$ (Z = Se, S, and Te) spinels. Thus, we theoretically investigated the electrical, magnetic, and transport properties of $SrCe_2Z_4$, where Z corresponds to Se, S, and Te, to realize their suitability for spintronic and energy harvesting device applications.

2. Computational study

The computations on $SrCe_2Z_4$ (Z = S, Se, Te) were performed utilizing the DFT-based FP-LAPW method within WIEN2k,[32] which is highly recommended for computing the structural, electronic, and magnetic characteristics. The structural characteristics were calculated using the PBE-GGA approximation.[33] This approximation calculates the structural findings exactly, but underestimates the electronic band gaps and electronic state calculations on which magnetic and thermoelectric characteristics depend. Therefore, the TB-mBJ potential[34] was used to compute these compositions' band structure and density of states. This versatile and accurate potential consumes less computational cost and is easier to handle than the hybrid functionals HSE06 and GGA + U potentials. The basis set comprises non-overlapping atomic spheres with muffin tin radii R_{MT} and an interstitial region having a plane wave expansion with wave vector k. The R_{MT} and K_{max} products are set to be 8. The plane wave cutoff value related to the Gaussian factor (G_{max}) was set to 16 during initialization. For the

expansion of the wave function, the maximum value of the angular momentum L_{max} was set as 10, as it is a dimensionless quantity. For a non-shifted 14 × 14 × 14 grid, a denser k-mesh is utilized for all physical properties. The default energy convergence criteria were set at 10^{-5} Ry. The BoltzTrap code[35] was used to compute the transport parameters of the studied compounds. The calculation of the electrical conductivity $\sigma_{\alpha\beta}(T)$ and Seebeck coefficient $S_{\alpha\beta}(T)$ as a function of temperature was performed using the following equations:

$$\sigma_{\alpha\beta}(T) = \frac{1}{\Omega}\int \sigma_{\alpha\beta}(\varepsilon)\left[\frac{\partial f(T)}{\partial \varepsilon}\right]\mathrm{d}\varepsilon \quad (1)$$

$$S_{\alpha\beta}(T) = \left(\frac{1}{eT\Omega\sigma_{\alpha\beta}(T)}\right)\int \sigma_{\alpha\beta}(\varepsilon)(\varepsilon-\mu)\left[\frac{\partial f(T)}{\partial \varepsilon}\right]\mathrm{d}\varepsilon \quad (2)$$

where Ω is the unit cell volume, $f(T)$ is the Fermi–Dirac distribution, e is the charge of the electron, and $\sigma_{\alpha\beta}(\varepsilon)$ is the transport distribution function as a function of energy, given by:

$$\sigma_{\alpha\beta}(\varepsilon) = e^2\sum_{i,k}\tau_{ik}v_\alpha(i,k)v_\beta(i,k)\delta(\varepsilon-\varepsilon_{i,k}) \quad (3)$$

3. Results and discussions

3.1. Structural properties

For spinel $SrCe_2Z_4$ (where Z is equal to S, Se, or Te), the face-centered cubic unit cell, having 8 formula units per unit cell, is depicted by a ball-stick model in Fig. 1(a). Sr, Ce, and Z have been represented with blue, brown, and yellow balls in this model, respectively. Sr is divalent (Sr^{2+}) and Ce is trivalent (Ce^{3+}), making them both non-transition cations, thereby classifying the structure as a normal spinel. The configurations have a space group of $Fd\bar{3}m$ (#227). In this unit cell, the atoms Sr, Ce, and Z have coordinates (0.125, 0.125, 0.125), (0.5, 0.5, 0.5), and (0.25, 0.25, 0.25), respectively. Each individual atom, Sr, Ce, and Z, has unique Wyckoff positions, such as 8a, 16d, and 32e,[36] respectively. Fig. 2(b) represents the polyhedral structure, where the anions form an FCC lattice. It can also be observed that the Sr atom occupies the tetrahedral void in SrZ_4, whereas Ce occupies the octahedral void in CeZ_6 in the FCC lattice.[37,38] So, from the above information, the coordination numbers of Sr, Ce, and Z in $SrCe_2Z_4$ are 4, 6, and 4, correspondingly.

The ground state energy (Ryd) and the volume (a.u.^{3}) in AFM and FM states were calculated and plotted using the Murnaghan equation of state.[39] Fig. 2 shows the two parabolic curves, with the red one representing the AFM state and the black curve representing the FM state. Fig. 2(a–c) demonstrates the volume optimization graphs of $SrCe_2S_4$, $SrCe_2Se_4$, and $SrCe_2Te_4$. In the AFM state, all compositions release less energy than in the FM state. Therefore, the FM state is energetically more favorable for all compositions. Among all these compositions, $SrCe_2Te_4$ has the highest lattice parameters and lowest ground state energy. Therefore, it is the most stable.[40]

The lattice constant a_0 (Å) can be calculated from Fig. 2. $SrCe_2Te_4$ has a higher lattice constant value (13.42 Å) [Table 1] because of the larger ionic radii of Te. The lattice constants for $SrCe_2S_4$ and $SrCe_2Se_4$ were 12.01 and 12.52 Å, respectively. As the bulk modulus B_0 (GPa) of the material is inversely proportional to the lattice constant, the bulk moduli decrease with the rise of the lattice constant. The value of B_0 was reported as 53.42 GPa for $SrCe_2S_4$, which declined to 42.76 and 33.42 GPa for $SrCe_2Se_4$ and $SrCe_2Te_4$, respectively.[41] The B_0 quantifies the hardness of a material by evaluating its resistance to uniform volumetric compression under applied pressure.[42] The FM states have higher thermodynamic stability due to their higher enthalpy (H_f) of formation, as the material releases more energy in this state.[43] From Table 1, the H_f value of $SrCe_2S_4$ is −2.20 eV, indicating its higher thermodynamic stability. The values of H_f for the Se and Te-based compositions are noted as −2.05 and −1.94 eV, respectively. The Curie temperatures of all

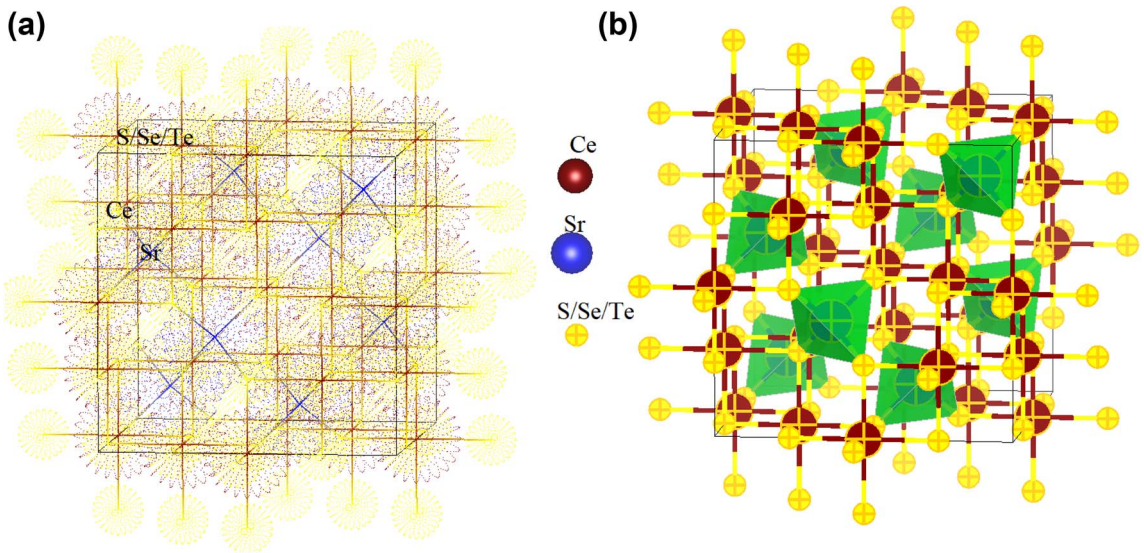

Fig. 1 (a) Illustration of the ball-stick model of the $SrCe_2Z_4$ crystal structure (with Z = S, Se, and Te), while (b) depicts the structure of the polyhedron.

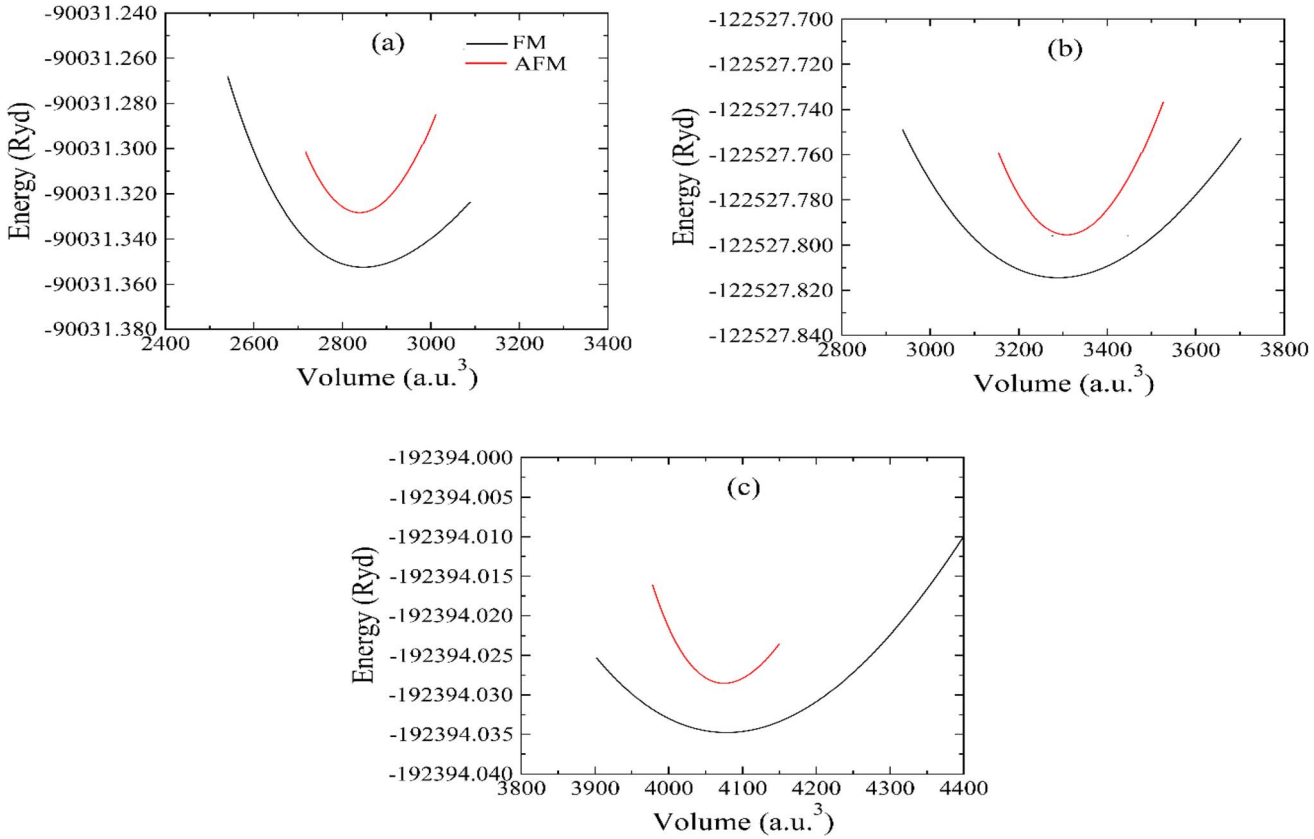

Fig. 2 Energy optimization trends for (a) $SrCe_2S_4$, (b) $SrCe_2Se_4$, and (c) $SrCe_2Te_4$.

Table 1 The computed structural parameters for $SrCe_2Z_4$ (Z = S, Se, Te)

Parameters	a_0 (Å)	B_0 (GPa)	H_f (eV)	T_c (K)	E_g (eV)	Ref.
$SrCe_2S_4$	12.01	53.42	−2.2	295	2.20	This work
HgY_2S_4	11.12	76.19	−8.64	—	1.20	44
$MgLu_2S_4$	10.82	78.03	—	—	2.60	45
MgY_2S_4	11.06	64.88	—	—	1.62	46
$LiCr_2S_4$	9.73	97.41	−1.18	—	1.40	47
$ZnMn_2S_4$	9.98	—	−2.86	—	1.55	48
$SrCe_2Se_4$	12.52	42.76	−2.05	302	1.71	This work
HgY_2Se_4	11.62	63.65	−6.88	—	0.60	44
$MgLu_2Se_4$	11.32	65.14	—	—	2.00	45
MgY_2Se_4	11.54	53.88	—	—	1.09	46
$LiCr_2Se_4$	10.24	78.86	—	—	1.10	47
$ZnMn_2Se_4$	10.57	—	−2.98	—	0.85	48
$SrCe_2Te_4$	13.42	33.42	−1.94	310	1.30	This work
$ZnMn_2Te_4$	11.34	—	−3.01	—	0.24	48

compositions are above room temperature, but $SrCe_2Te_4$ has a higher Curie temperature (310 K). The Curie temperature being near room temperature positions these materials as promising aspirants for energy-efficient data erasing and writing under manageable thermal conditions.[36]

3.2. Electronics properties

The electrical properties, such as the density of states (DOS) and the band structure (BS), are critical computations to evaluate the composite's potential for optical applications. Sr-based spinels exhibit exciting electronic properties that verify their FM nature. The TB-mBJ potential is used as the theoretical approach to achieve an accurate bandgap value because of its ability to accurately predict BS, as investigated in previous studies.[49] The BS properties of three compositions, $SrCe_2S_4$, $SrCe_2Se_4$, and $SrCe_2Te_4$, are demonstrated in Fig. 3(a–c). The dashed line separating the conduction (CB) and the valence bands (VB) represents the Fermi energy (E_f). In all compositions, the VB maxima and CB minima lie on the same symmetry point, showing the direct bandgap nature of these materials.[50] In Fig. 3(a) and (c), in the S↑ orientation, the energy states are close to the E_f, indicating semiconducting behavior. In contrast, the S↓ channel shows the insulating behavior due to a large bandgap separating the states of the VB and CBs. This suggests their FM nature with complete spin polarization. Overall, the BS of $SrCe_2S_4$ and $SrCe_2Te_4$ indicates that the material behaves as an FM semiconductor.[51] The spin-polarized behavior of both examined compositions is calculated by utilizing this formula:

$$P = \frac{\mathrm{Do}^{\uparrow}(E_f) - \mathrm{Do}_{\downarrow}(E_f)}{\mathrm{Do}^{\uparrow}(E_f) + \mathrm{Do}_{\downarrow}(E_f)} \times 100 \quad (4)$$

where $\mathrm{Do}^{\uparrow}(E_f)$ and $\mathrm{Do}^{\uparrow}(E_f)$ signify the DOS at the E_f for the S↑ and S↓ channels, correspondingly.[52] Due to the energy states being slightly above the E_f, the $SrCe_2Se_4$ in the S↑ channel exhibits a metallic nature, as illustrated in Fig. 3(b). The S↓

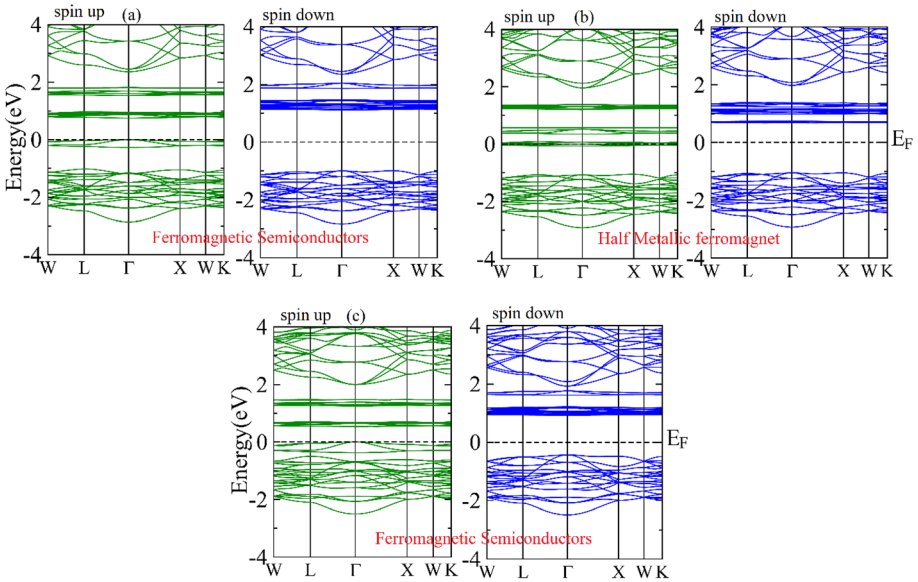

Fig. 3 The band structures in both the spin-up and spin-down channels: (a) $SrCe_2S_4$, (b) $SrCe_2Se_4$, and (c) $SrCe_2Te_4$.

channel shows insulating behavior because the Fermi level lies within these bands.[53] So, the overall nature of $SrCe_2Se_4$ is half-metallic. In Fig. 3(c), the energy difference between the VB and CB indicates that the E_g of $SrCe_2Te_4$ is minimal. Due to the half-metallic nature, the E_g of $SrCe_2Se_4$ is not considered.

The total DOS and the partial DOS for each atom are calculated to provide a detailed explanation of the mechanism of ferromagnetism.[54] Fig. 4 illustrates the TDOS and PDOS of the $SrCe_2S_4$ composition. The TDOS reflects the electronic BS, and the energy states are shown as peaks. In Fig. 4, the TDOS reflects the combined contributions of all atoms and their corresponding valence orbitals, with VB on the left side and CB on the other side of the Fermi level. According to the PDOS plot, the VB edge at the Fermi energy is composed of 4f—Ce states and 3p—S states together, while 5s—Sr and 3p—S states firmly hybridize in the VB in the energy range from −2.8 eV to −1 eV. In the CB, near the E_f, 4f—Ce has a significant contribution, ranging from 0.5 to 1.95 eV. So, Ce's overall PDOS has made a substantial contribution to TDOS.

In contrast to earlier compositions, $SrCe_2Se_4$ demonstrates a half-metallic ferromagnetic nature, as demonstrated by its band structure and DOS analysis. The TDOS and PDOS plots for this composition are highlighted in Fig. 5, which indicates that the 4f—Ce states play a significant role close to the Fermi level,

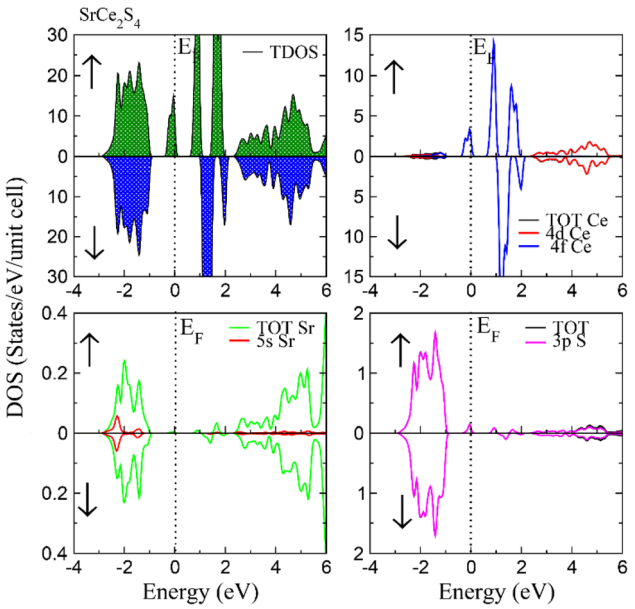

Fig. 4 The TDOS and PDOS of $SrCe_2S_4$ in the spin-up and spin-down channels.

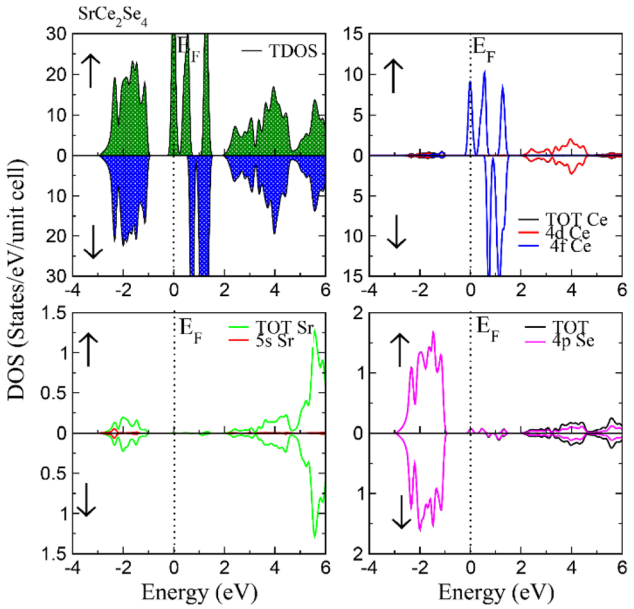

Fig. 5 The TDOS and PDOS of $SrCe_2Se_4$ in the spin up and spin down channels.

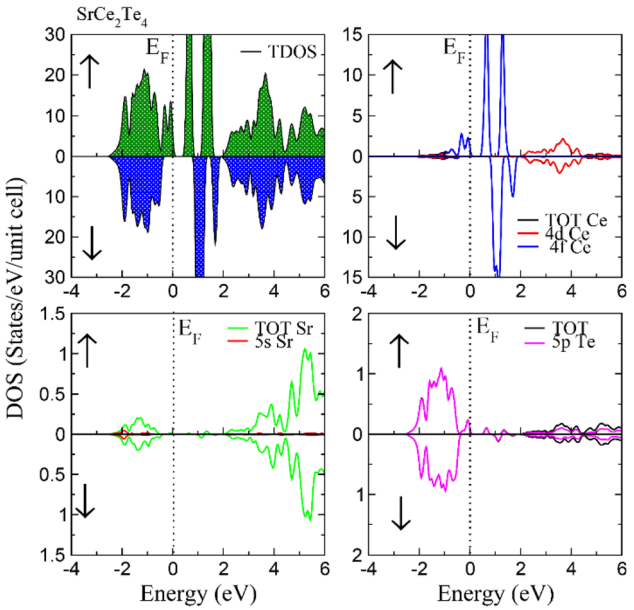

Fig. 6 The TDOS and PDOS of $SrCe_2Te_4$ in the spin up and spin down channels.

crossing the E_f between −0.2 eV and 0.2 eV and causing the metallic behavior in the spin-up channel. On the other hand, the 4p—Se states exhibit insulating properties and contribute little at E_f, but are essential in the valence band (VB) between −2.9 eV and −1 eV. Furthermore, these states lie in the range of 2–6 eV in the conduction band. The unique half-metallic behavior is reinforced by the fact that Ce makes the most significant overall contribution to the TDOS. The interaction of energy states is responsible for this behavior, which aligns with observations in similar materials and highlights the importance of composition in controlling electronic properties.[55]

Fig. 6 illustrates the TDOS and PDOS for $SrCe_2Te_4$. Like the other two compositions, the Ce element has the maximum involvement in the development of the TDOS. In this case, the energy states near the E_F, extending from −1 eV to the Fermi level, show that a greater number of peaks are present compared to the other two compositions, and there is a slight variance between the highest value of the VB and the minimum value of the CB, indicating the lowest E_g of $SrCe_2Te_4$.

3.3. Magnetic properties

The magnetic properties reflect how the material responds to an external magnetic force field. The magnetic nature of the substance can be conceptualized in terms of direct Δ_x(f) and indirect Δ_x(pf) exchange energies, crystal field stabilization energy Δ_{CF}, and exchange constants $N_o\alpha$ and $N_o\beta$.[56] The geometry of f-orbitals is more complex than that of d orbitals, so the crystal field stabilization energy, ΔCF, cannot be calculated for compositions containing f-block metal cations. For a material to exhibit an FM nature, the value of the direct exchange energy Δ_x(f) must be higher than the stabilization energy.[57] The Δ_x(f) exhibits negative values of −0.32, −1.047, and −0.36 eV for $SrCe_2Z_4$ (Z = S, Se, Te), where $SrCe_2S_4$ and $SrCe_2Te_4$ show ferromagnetic semiconducting behavior and $SrCe_2Se_4$ exhibits a half-metallic nature. The negative sign usually indicates the material's ferromagnetic ordering, confirming its ferromagnetic nature.[58] This unexpected ferromagnetism is due to the dominance of indirect exchange interaction, such as double exchange or the super exchange mechanism.[59] The formula can calculate the value of Δ_x(f) as $\Delta_x(f) = \Delta\backslash(f)^{\downarrow} - \Delta(f)^{\uparrow}$.[60] The indirect exchange of energy Δ_x(pf) is produced by the hybridization between p-block chalcogens (S, Se, Te) and f-block Ce. We can calculate the Δ_x(pf) from only the VB maximum S and the S channel's maximum peaks. The value of the indirect exchange is negative, indicating the FM behavior in the S↓ channel for $SrCe_2S_4$, $SrCe_2Se_4$, and $SrCe_2Te_4$, showing their intense spin polarization.[61] All the calculated values are presented in Table 3.

The interaction in which electrons from CBs exchange with the localized MM is referred to as the exchange constant $N_o\alpha$. The exchange interaction involving holes from the VB and the localized MM is categorized by the exchange constant $N_o\beta$. The following formula can be used to calculate the $N_o\alpha$ and $N_o\beta$:

$$N_o\alpha = \frac{\Delta E_c}{\langle xS \rangle} \quad (5)$$

$$N_o\beta = \frac{\Delta E_v}{\langle xS \rangle} \quad (6)$$

From Table 2, we can observe the value of $N_o\alpha$ and $N_o\beta$. Here, $\Delta E_c = E_c^{\downarrow} - E_c^{\uparrow}$ indicates the splitting at the CB edge, and $\Delta E_v = E_v^{\downarrow} - E_v^{\uparrow}$ represents the splitting at the VB edge.[57] Table 2 shows that the obtained results of $N_o\alpha$ and $N_o\beta$ for $SrCe_2Z_4$ (Z = S, Se, Te) are negative and induce intense spin polarization, leading to the FM order of $SrCe_2S_4$ and $SrCe_2Te_4$. With the influence of the spin-exchange interactions and electronic structure, $SrCe_2Se_4$ shows half-metallic ferromagnetism.[62] From the exchange constant equations, the splitting of the CB edge depends on s-f hybridization among the s-Sr and f-Ce orbitals. In contrast, VB maxima splitting relies on the p–f coupling between p–Z (Z = S, Se, Te) and f-Ce orbitals.[59] The total amount of MM can be determined based on the number of unpaired electrons in the f-orbitals.[55] From Table 2, the value of total MM for all three compositions is 4 μ_B, which indicates that all magnetic spins are equally aligned and have significant

Table 2 List of the computed aspects (Δ_x(pf), Δ_x(f), $N_o\beta$, $N_o\alpha$, Sr, Ce, *X*, Int, and the total magnetic moments) for $SrCe_2Z_4$ (Z = S, Se, Te)

Compositions	Δ_x(f) (eV)	Δ_x(pf) (eV)	$N_o\alpha$	$N_o\beta$	Total (μ_B)	Int (μ_B)	Sr (μ_B)	*X* (μ_B)	Ce (μ_B)
$SrCe_2S_4$	−0.32	−0.945	−1.89	−0.732	4	0.151	0.007	0.005	0.952
$SrCe_2Se_4$	−1.047	−0.75	−1.056	−0.959	4	0.148	0.01	0.012	0.983
$SrCe_2Te_4$	−0.36	−0.45	−1.463	−0.403	4	0.154	0.008	0.04	0.97

magnetic order, leading to intense spin polarization. The small value of Sr and the considerable value of Ce indicate that Ce makes a greater contribution to the overall composition $SrCe_2Z_4$. The value of interstitial MM suggests that the regions between the atomic gaps also contribute to the overall magnetic response of these materials.

3.4. Transport properties

Thermoelectric materials can facilitate heat transformation into electrical power, and their efficiency is measured in the context of the power factor (PF) or Figure of Merit (ZT). These performance-determining parameters are calculated in terms of the thermal conductivity (κ), electrical conductivity (σ), Seebeck coefficient (S), power factor ($S^2\sigma$), and the ZT.[61,62] The numerical values of these parameters are critical in deciding the applications of materials. Fig. 7 shows how different thermoelectric parameters change with T for $SrCe_2S_4$, $SrCe_2Se_4$, and $SrCe_2Te_4$. Fig. 7(a) demonstrates the graph between σ and T, indicating that σ rises with temperature, attributed to the increase in the thermally generated charge carrier concentration and their mobility.[63] Among the compositions studied, $SrCe_2Te_4$ showed the highest σ values because of its smaller E_g, leading to higher carrier concentration and mobility.

Thermal conductivity (κ) measures how much heat can be transferred through a material. There are two parts of κ; electronic (κ_e) and lattice thermal conductivity (κ_L).[62] Here, we can report the κ_e because the lattice part is beyond the computational capabilities of the BoltzTraP function. The variation of κ_e with T has been presented in Fig. 7(b), indicating that κ_e increases with T because more electrons can be thermally excited from the VB to the CB at the elevated temperature.[43] This leads to higher carrier concentration and higher mobility, which increases the κ_e.[63]

Fig. 7(c) shows how the Seebeck coefficient changes with T. The Seebeck coefficient measures how much voltage is produced due to a 1 K temperature change in any material.[62]

$$S = \frac{\Delta V}{\Delta T} \tag{7}$$

At lower temperatures, carrier concentrations are lower, leading to a higher S. So, as the T increases, the S decreases because of an increase in the carrier concentration and higher mobility. Higher mobility causes a reduction in voltage production, leading to a lower S at higher T.[56] The S value of $SrCe_2S_4$ is larger than that of other compositions because of its lower carrier concentration, leading to a higher S.[63] Fig. 7(b) shows the temperature-dependent electronic part of the thermal conductivity for $SrCe_2Z_4$. It is clear that $SrCe_2Te_4$ showed a higher value of thermal conductivity, which is attributed to a higher carrier concentration, higher mobility, and less phonon scattering as compared to other compositions. ZT and PF are key parameters that are employed to govern the thermoelectric efficiency of any material. The value of PF depends upon the value of σ and the S, and can be expressed as:[60]

$$\mathrm{PF} = \frac{S^2\sigma}{\tau} \tag{8}$$

From Fig. 7(d), we can observe that the reported results of PF confirm the slight upsurges with the elevation of T. The value of PF will be higher when the product of σ and S square is the maximum value in semiconductors.[60] In Fig. 8(a), it has been observed that there is minimal phonon scattering at lower T, resulting in the usual scattering where the momentum and energy are conserved.[64] This leads to the elastic scattering of phonons, and there is thus a greater κ_L at the start. However, as T continues to rise, the scattering becomes more pronounced,

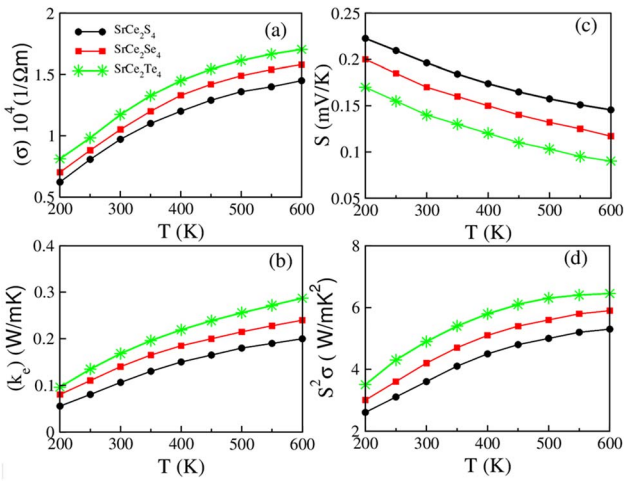

Fig. 7 Temperature-dependent variation of (a) σ, (b) k_e, (c) S, and (d) $S^2\sigma$ for $SrCe_2Z_4$.

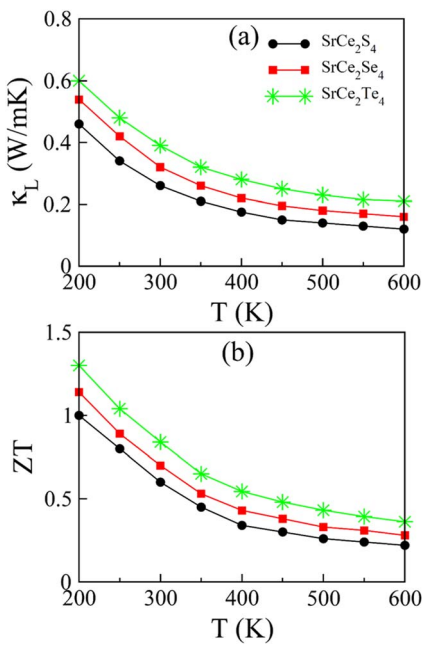

Fig. 8 Temperature-dependent variation of (a) k_L and (b) ZT for $SrCe_2Z_4$.

Table 3 Thermoelectric parameters of $SrCe_2Z_4$ (where Z = S, Se, Te) at room temperature

Compositions	σ/τ (1/Ωm × 10^4)	κ_e/τ (W mK^{-1})	S (mV K^{-1})	PF (W mK^{-2})	ZT	Ref.
$SrCe_2S_4$	0.97	0.106	0.14	3.6	0.60	This work
HgY_2S_4	24.1	0.49	223.36	1.20	0.72	44
$MgLu_2S_4$	1.91	0.46	245.6	1.15	0.74	45
MgY_2S_4	1.381	0.334	242.567	—	0.731	46
$LiCr_2S_4$	0.88	0.90	−94.43	0.79×10^{-3}	—	47
$ZnMn_2S_4$	9.48	6.61	7.46	0.05×10^{-3}	—	48
$SrCe_2Se_4$	1.05	0.14	0.17	4.20	0.70	This work
HgY_2Se_4	17.6	0.40	239.48	1.01	0.75	44
$MgLu_2Se_4$	1.82	0.42	239.1	1.04	0.75	45
MgY_2Se_4	1.150	0.248	230.585	—	0.739	46
$LiCr_2Se_4$	1.58	1.67	−64.20	0.66	—	47
$ZnMn_2Se_4$	11.58	8.11	6.60	0.05×10^{-3}	—	48
$SrCe_2Te_4$	1.17	0.168	0.196	4.9	0.94	This work
$ZnMn_2Te_4$	12.10	8.65	10.07	0.12×10^{-3}	—	48

due to which the energy and momentum are no longer conserved, causing a reduction in κ_L.[54] From Table 3, the value of PF for $SrCe_2Te_4$ is observed to be 4.90 W mK^{-2} at RT. The value of ZT may be determined based on κ, S, and σ, employing the expression below.[60]

$$ZT = \frac{\sigma S^2 T}{\kappa} \quad (9)$$

From Fig. 8(b), we can observe that with an increase in T, the value of ZT decreases due to the combined effect of κ and S.[57,60] At low T, the ZT value is higher due to the larger value of S and σ. So, when the T rises, the value of ZT decreases because of the increase of κ.[64,65] At higher T, the S and σ also decrease, resulting in a lower value of ZT. The calculated values of all thermoelectric parameters for $SrCe_2S_4$, $SrCe_2Se_4$, and $SrCe_2Te_4$ at room temperature are listed in Table 3. These values provide a quick reference for the thermoelectric performance of the studied material at room temperature.[66] The large ZT at room temperature ensures their applications for thermoelectric generators, effectively transforming heat into electrical power.[67]

4. Conclusion

In summary, the structural, electrical, magnetic, and thermoelectric aspects of $SrCe_2Z_4$ (Z = S, Se, Te) have been systematically explored to validate their applicability for energy harvesting and spintronic implementations. In optimization, the released energy upon transition to the FM state and negative formation energy collectively ensured their structural and thermodynamic stability in FM states. The analysis of the spin-polarized band structure demonstrated the half-metallic ferromagnetic behavior of $SrCe_2Se_4$ and the ferromagnetic semiconducting nature of $SrCe_2S_4$ and $SrCe_2Te_4$. The Heisenberg model analysis showed that the Curie temperature ranged from 295–310 K, which is above room temperature, indicating ferromagnetism in these spinels. The DOS confirmed that the strong coupling of p-orbitals of chalcogens and the 4f-states of Ce governed the exchange mechanism of electrons, resulting in ferromagnetism. The investigation of direct and indirect exchange energy, along with exchange constants, ascertained the dropping of energy of the FM state and stabilized ferromagnetism. Moreover, Ce's magnetic moment distribution to the Sr and S/Se/Te sites was attributed to the electron exchange interactions, rather than the formation of a magnetic cluster of Ce ions. Finally, the bigger electrical and ultra-low thermal conductivity improved the power factor and figure of merit performances. The ZT value of 0.90 at room temperature for $SrCe_2Te_4$ showcased its potential for thermoelectric devices.

Conflicts of interest

There is no conflict to declare.

Data availability

All data included in this study may be obtained from the corresponding author on reasonable request.

Acknowledgements

This research was funded by the Princess Nourah bint Abdulrahman University Researchers Supporting Project number (PNURSP2025R7), Princess Nourah bint Abdulrahman University, Riyadh, Saudi Arabia. The authors express their gratitude to the Deanship of Scientific Research at Northern Border University, Arar, KSA, for funding this research work through the project number "NBU-FFR-2025-2985-18".

References

1 N. Rahman, A. Azzouz-Rached, M. Husain, B. M. Al-Khamiseh, K. M. Abualnaja, G. Alosaimi, V. Tirth, H. Alqahtani, A. Algahtani, T. Al-Mughanam and S. Belhachi, Impact of samarium on magnetic and optoelectronic properties of magnesium-based $MgSm_2X_4$ (X= S and Se) spinels for spintronics, *PLoS One*, 2024, **19**(8), e0309388.

2 S. Sohail, M. Irfan, Q. Ain, F. A. Ibrahim, M. S. Hamdy, S. A. Issa and H. M. Zakaly, First principles computation of exchange mechanism, radiation shielding, and physical properties of $FeCu_2SnX_4$ (X= S, Se, Te): Transitions metal based chalcogenides for spintronic and energy storage system applications, *Mater. Sci. Semicond. Process.*, 2025, **190**, 109303.

3 G. Datt, Spinel ferrite-based heterostructures for spintronics applications, *InFerrite Nanostructured Magnetic Materials*, Woodhead Publishing, 2023, 1, pp. 747–773.

4 M. Robail, N. A. Noor, M. W. Iqbal, H. Ullah, A. Mahmood, M. A. Naeem and Y. H. Shin, Comprehensive study of ferromagnetic $MgNd_2X_4$ (X= S, Se) spinels for spintronic and solar cells device applications, *Ceram. Int.*, 2022, **48**(2), 2385–2393.

5 M. M. Rahman, N. Hasan, S. Tabassum, M. H. Rashid, M. H. Rashid and M. Arifuzzaman, Bi^{3+} doped nanocrystalline Ni–Co–Zn spinel ferrites: Tuning of physical, electrical, dielectric and magnetic properties for advanced spintronics applications, *Ceram. Int.*, 2024, **50**(21), 44585–44597.

6 R. A. Ribeiro, S. R. De Lazaro and S. A. Pianaro, Density functional theory applied to magnetic materials: Mn_3O_4 at different hybrid functionals, *J. Magn. Magn. Mater.*, 2015, **391**, 166–171.

7 S. Nazir, N. A. Noor, R. Sharma, M. I. Rasheed, M. A. Yasir, M. Aslam and Y. M. Alanazi, Study of the spin-polarized electronic, exchange constant, and thermoelectric characteristics of spinels $LiFe_2(O/S)_4$ for spintronic and energy-harvesting applications, *J. Phys. Chem. Solids*, 2024, **189**, 111975.

8 N. A. Noor, M. Tahir, M. A. Khan, S. Niaz, H. Ullah, R. Neffati and R. Sharma, Theoretical study of rare earth in the spinels chalcogenide $MgCe_2Z_4$ (Z= S, Se) for spintronic and thermoelectric applications, *Mater. Sci. Semicond. Process.*, 2023, **163**, 107563.

9 S. M. Yakout, Spintronics: future technology for new data storage and communication devices, *J. Supercond. Nov. Magnetism*, 2020, **33**(9), 2557–2580.

10 M. Ishfaq, S. A. Aldaghfag, M. Z. Kazim, S. Rauf, M. Yaseen and A. Dahshan, Comprehensive DFT investigation of X_2MgSe_4 (X= Dy, Tm) spinels for opto-spintronic and thermoelectric devices, *Phys. Scr.*, 2024, **99**(4), 045908.

11 S. Nazir, N. A. Noor, A. Hussain, S. Naseem, S. Riaz, A. Laref, S. Mumtaz and A. Ibrahim, DFT study of rare-earth ferromagnetic spinels $HgNd_2Z_4$ (Z= S, Se) for spintronics applications, *J. Rare Earths*, 2024, **43**(6), 1228–1237.

12 H. A. Alburaih, S. Nazir, N. A. Noor, A. Laref and R. Sharma, Study of the Influence of Electron Spin in Ferromagnetism and Thermoelectric Characteristics of $CdTm_2Y_4$ (Y= S, Se) Spinels for Spintronic Applications, *ACS Omega*, 2023, **8**(43), 40341–40350.

13 I. Tariq, M. Yaseen, S. A. Aldaghfag and A. Aziz, Investigation of X_2CdS_4 (X= Dy, Tm) spinels for energy harvesting and spintronic applications, *J. Solid State Chem.*, 2023, **320**, 123846.

14 L. Cario, B. Corraze and E. Janod, Physics and Chemistry of Chalcogenide Quantum Materials with Lacunar Spinel Structure, *Chem. Mater.*, 2025, **37**(2), 532–550.

15 K. E. Sickafus, J. M. Wills and N. W. Grimes, Structure of spinel, *J. Am. Ceram. Soc.*, 1999, **82**(12), 3279–3292.

16 R. J. Hill, J. R. Craig and G. V. Gibbs, Systematics of the spinel structure type, *Phys. Chem. Miner.*, 1979, **4**(4), 317–339.

17 K. Righter, W. P. Leeman and R. L. Hervig, Partitioning of Ni, Co and V between spinel-structured oxides and silicate melts: Importance of spinel composition, *Chem. Geol.*, 2006, **227**(1–2), 1–25.

18 N. Zhao, Y. F. Zhu and Q. Jiang, Novel electronic properties of two-dimensional As_xSb_y alloys studied using DFT, *J. Mater. Chem. C*, 2018, **6**(11), 2854–2861.

19 A. Ramzan, M. Y. Sofi, M. Ishfaq-ul-Islam, M. S. Khan and M. A. Khan, Half-metallic ferromagnetism and thermoelectric-efficient behavior in chalcogenide spinels $MgNi_2X_4$ (X= S, Se): a first-principles approach, *RSC Adv.*, 2025, **15**(29), 24002.

20 A. Gilani, S. A. Aldaghfag and M. Yaseen, Magnetic, optical, electronic, structural and thermoelectric features of A_2MgS_4 (A= Sm, Tb): A DFT study, *J. Phys. Chem. Solids*, 2023, **175**, 111208.

21 M. Hassan, S. A. Rouf, A. S. Alofi, Q. Mahmood, A. Ishfaq, M. mana AL-Anazy, A. S. Alshomrany, M. F. Rahman and E. SayedYousef, Impact of terbium (Tb) on ferromagnetism and thermoelectric behaviour of spinels $MgTb_2(S/Se)_4$ for spintronic, *Mater. Sci. Eng., B*, 2024, **300**, 117110.

22 H. A. Alburaih, N. A. Noor, M. Bououdina, H. Ullah, A. Laref and R. Sharma, First-principle study of Mg-based rare earth spinels $MgSm_2Y_4$ (YS, Se) for spintronic and thermoelectric devices, *Mater. Chem. Phys.*, 2024, **313**, 128756.

23 K. Manjunatha, V. J. Angadi, R. A. Ribeiro, M. C. Oliveira, S. R. De Lázaro, M. R. Bomio, S. Matteppanavar, S. Rayaprol, P. D. Babu and U. M. Pasha, Structural, electronic and magnetic properties of Sc 3+ doped $CoCr_2O_4$ nanoparticles, *New J. Chem.*, 2020, **44**(33), 14246–14255.

24 S. Maqsood, M. A. Javed, S. Mumtaz and M. K. Al-Sadoon, Computational study of Cd-based chalcogenide spinels $CdSm_2(S/Se)_4$ for spintronic applications, *Chalcogenide Lett.*, 2024, **21**(6), 449–458.

25 N. A. Noor, F. Nasrullah, I. M. Moussa and S. Mumtaz, Mechanical, magnetic, and electronic characteristics of Sm-based chalcogenides for spintronics and device applications, *Chalcogenide Lett.*, 2024, **21**(5), 413–421.

26 N. A. Kattan, S. A. Rouf, H. D. Alkhaldi, M. Hassan, S. Al-Qaisi, A. I. Aljameel, H. Albalawi, I. Boukhris, Q. Mahmood and U. Mumtaz, Study of Half Metallic Ferromagnetism and Thermoelectric Properties of the Spinels $MgCo_2(S/Se)_4$ for Spintronic and Energy Harvesting, *J. Inorg. Organomet. Polym. Mater.*, 2025, **35**(2), 724–737.

27 H. Albalawi, A. Azazi, Q. Mahmood, N. A. Kattan, S. Al-Qaisi, G. Murtaza, F. Ercan, S. Bouzgarrou and M. Jadan, Study of role of spin in ferromagnetism and thermoelectric characteristics of spinel chalcognides $MgEr_2(S/Se)_4$ for

spintronic and clean energy, *J. Solid State Chem.*, 2023, **324**, 124128.

28 H. Khushi, S. Nazir, N. A. Noor, A. Mahmood, Y. M. Alanazi and S. Mumtaz, First-Principles Simulation of Ferromagnetic $CdHo_2Y_4$ (Y= S, Se) Spinels for Energy Storage Applications, *J. Electrochem. Soc.*, 2023, **170**(6), 060544.

29 R. Ramzan, N. A. Noor, M. W. Iqbal, M. Asghar, A. Khan, A. Dahshan and A. Alqahtani, Ab-initio study of half-metallic ferromagnetism and transport characteristics of MgV_2S/Se_4 spinels for spintronics and thermoelectric applications, *Phys. Scr.*, 2022, **97**(8), 085821.

30 M. Bilal, N. A. Noor, M. W. Iqbal, M. A. Khan, S. Niaz, A. Sohail, Y. M. Alanazi, S. Aftab and R. Neffati, New magnesium based half-metallic ferromagnetic chalcogenide $MgFe_2Z_4$ (Z= S, Se) spinels; a promising materials for spintronic applications, *Phys. Scr.*, 2022, **97**(12), 125815.

31 H. A. Alburaih, Probing of Ferromagnetism and Electronic transport characteristics of Rare-earth-based $CdEr_2X_4$ (X= S, Se) Spinels for Spintronic and Energy Harvesting Applications, *J. Alloys Compd.*, 2021, **876**, 159806.

32 J. P. Perdew, A. Ruzsinszky, G. I. Csonka, O. A. Vydrov, G. E. Scuseria, L. A. Constantin, X. Zhou and K. Burke, Restoring the density-gradient expansion for exchange in solids and surfaces, *Phys. Rev. Lett.*, 2008, **100**(13), 136406.

33 P. Blaha, K. Schwarz, G. K. Madsen, D. Kvasnicka and J. Luitz, wien2k. An augmented plane wave+ local orbitals program for calculating crystal properties, *Phys. Rev. B:Condens. Matter Mater. Phys.*, 2001, **60**(1), 155–169.

34 F. Tran and P. Blaha, Accurate Band Gaps of Semiconductors and Insulators with a Semilocal Exchange-Correlation Potential, *Phys. Rev. Lett.*, 2009, **102**(22), 226401.

35 G. K. Madsen and D. J. Singh, BoltzTraP. A code for calculating band-structure dependent quantities, *Comput. Phys. Commun.*, 2006, **175**(1), 67–71.

36 A. Liang, Z. Li, S. Zhang, S. Sun, S. Liu, C. Chen, H. Yang, S. Cui, S. K. Mo, S. Yang and Y. Li, Electronic origin of half-metal to semiconductor transition and colossal magnetoresistance in spinel $HgCr_2Se_4$, *Phys. Rev. B*, 2023, **107**(19), 195114.

37 J. M. Hastings and L. M. Corliss, Magnetic structure of manganese chromite, *Phys. Rev.*, 1962, **126**(2), 556.

38 N. A. Noor, M. Hassan, M. Rashid, S. M. Alay-e-Abbas and A. Laref, Systematic study of elastic, electronic, optical and thermoelectric properties of cubic $BiBO_3$ and $BiAlO_3$ compounds at different pressure by using ab-initio calculations, *Mater. Res. Bull.*, 2018, **97**, 436–443.

39 F. D. Murnaghan, The compressibility of media under extreme pressures, *Proc. Natl. Acad. Sci. U. S. A.*, 1944, **30**(9), 244–247.

40 S. M. Hosseini, Structural, electronic and optical properties of spinel $MgAl_2O_4$ oxide, *Phys. Status Solidi B*, 2008, **245**(12), 2800–2807.

41 S. S. Shah, G. Murtaza, S. Khan, S. Muhammad, A. Yar and M. W. Ashraf, First Principles Investigation of Electronic, Optical, and Magnetic Properties of $MgYb_2X_4$ (X= S, Se, Te), *J. Supercond. Novel Magn.*, 2023, **36**(1), 263–273.

42 T. Blachowicz, and A. Ehrmann, *Spintronics: Theory, Modelling, Devices*, Walter de Gruyter GmbH & Co KG, 2024.

43 M. Nazar, S. A. Aldaghfag, M. Yaseen, M. Ishfaq, R. A. Khera, S. Noreen and M. H. Abdellattif, First-principles calculations to investigate structural, magnetic, optical, electronic and thermoelectric properties of X_2MgS_4 (X= Gd, Tm) spinel sulfides, *J. Phys. Chem. Solids*, 2022, **166**, 110719.

44 G. M. Mustafa, S. Saba, N. A. Noor, A. Laref, M. Abd El-Rahman, Z. Farooq, R. B. Behram and Z. Ullah, First-principles calculations to investigate HgY_2S/Se_4 spinel chalcogenides for optoelectronic and thermoelectric applications, *J. Mater. Res. Technol.*, 2023, **22**, 97–106.

45 G. M. Mustafa, N. A. Noor, M. W. Iqbal, M. Sajjad, M. A. Naeem, Q. Mahmood, H. M. Shaikh, A. Mahmood and W. Al-Masry, Study of optoelectronic and transport properties of $MgLu_2Z_4$ (Z= S, Se) spinels for optoelectronic and energy harvesting applications, *Mater. Sci. Semicond. Process.*, 2021, **121**, 105452.

46 M. Zanib, N. A. Noor, M. A. Iqbal, I. Mahmood, A. Mahmood, S. M. Ramay, N. Y. Al-Garadi and T. Uzzaman, Density functional theory study of electronic, optical and transport properties of magnesium based MgY_2Z_4 (Z= S and Se) spinels, *Curr. Appl. Phys.*, 2020, **20**(10), 1097–1102.

47 M. U. Sohaib, N. A. Noor, M. Manzoor, A. Laref and A. Dahshan, Physical characteristics of ferromagnetic Cr-based $LiCr_2X_4$ (X= S, Se) spinels for spintronic and solar energy devices applications, *Eur. Phys. J. Plus*, 2022, **137**(5), 1–8.

48 N. A. Noor, M. Rashid, G. M. Mustafa, A. Mahmood, W. Al-Masry and S. M. Ramay, Zinc based chalcogenides $ZnMn_2X_4$ (X= S, Se, Te) as promising spintronic and sustainable energy materials: Ab-initio DFT investigations, *J. Alloys Compd.*, 2021, **856**, 157198.

49 P. Govindaraj, K. Murugan and K. Venugopal, Thermoelectric power factor of $MnSb_2X_4$ (X= S, Se) spinel chalcogenides–A DFT study, *Comput. Mater. Sci.*, 2022, **215**, 111758.

50 S. Elhadfi, H. Kerrai, J. Chenouf, Z. Arbaoui, B. Fakrach, A. H. Rahmani and H. Chadli, Optoelectronic and thermoelectric characterization of MgX_2S_4 (X= Ga, In) Spinels: A DFT approach for energy Applications, *Vacuum*, 2025, 114696.

51 G. Murtaza, R. Khenata, S. Mohammad, S. Naeem, M. N. Khalid and A. Manzar, Structural, elastic, electronic and optical properties of $CsMCl_3$ (M= Zn, Cd), *Phys. B*, 2013, **420**, 15–23.

52 A. Walsh, S. H. Wei, Y. Yan, M. M. Al-Jassim, J. A. Turner, M. Woodhouse and B. A. Parkinson, Structural, magnetic, and electronic properties of the Co-Fe-Al oxide spinel system: Density-functional theory calculations, *Phys. Rev. B Condens. Matter*, 2007, **76**(16), 165119.

53 U. G. Jong, C. J. Yu, Y. H. Kye, S. H. Choe, J. S. Kim and Y. G. Choe, Anharmonic phonons and phase transitions in the vacancy-ordered double perovskite Cs_2SnI_6 from first-principles predictions, *Phys. Rev. B*, 2019, **99**(18), 184105.

54 H. S. Saini, M. Singh, A. H. Reshak and M. K. Kashyap, Variation of half metallicity and magnetism of $Cd_{1-x}Cr_xZ$ (Z= S, Se and Te) DMS compounds on reducing dilute limit, *J. Magn. Magn Mater.*, 2013, **331**, 1–6.

55 A. A. Mousa, S. M. Al Azar, S. S. Essaoud, K. Berarma, A. Awad, N. T. Mahmoud, E. K. Jaradat and M. S. Abu-Jafar, Structural, Elastic, Electronic, Magnetic, and Thermoelectric Characteristics of $MgEu_2X_4$ (X= S, Se) Spinel Compounds: Ab-Initio Calculations, *Phys. Status Solidi B*, 2022, **259**(10), 2200191.

56 N. A. Noor, M. A. Majeed, M. A. Khan, S. Niaz, M. W. Iqbal, T. Abbas and A. Dahshan, Analysis of Mg-based spinels $MgGd_2X_4$ (X= S, Se) for spintronic and thermoelectric device applications: Ab-initio calculations, *Mater. Sci. Semicond. Process.*, 2022, **149**, 106861.

57 M. Salama, H. Kerrai, E. M. Jalal, H. Saadi, E. B. Choubabi and M. El Bouziani, Probing the Structural, Electronic, and Optical Properties of Ferromagnetic Rare-Earth-Based $CdEr_2S_4$ Spinel for Energy Harvesting Applications, *J. Inorg. Organomet. Polym. Mater.*, 2025, **21**, 1–9.

58 X. Yang, C. Wang, R. Lu, Y. Shen, H. Zhao, J. Li, R. Li, L. Zhang, H. Chen, T. Zhang and X. Zheng, Progress in measurement of thermoelectric properties of micro/nano thermoelectric materials: A critical review, *Nano Energy*, 2022, **101**, 107553.

59 H. Raebiger, A. Ayuela and R. M. Nieminen, Intrinsic hole localization mechanism in magnetic semiconductors, *J. Phys.: Condens. Matter*, 2004, **16**(41), L457.

60 M. Sameeullah, M. Ishfaq, S. A. Aldaghfag, M. Yaseen, M. Nazar and A. Dahshan, Magnetic, optoelectronic, and thermoelectric characteristics of Ln_2MnSe_4 (Ln= Yb, Lu) spinel chalcogenides: a DFT investigation, *J. Solid State Chem.*, 2023, **326**, 124238.

61 Tritt T. M., editor. *Thermal conductivity: theory, properties, and applications*, Springer Science & Business Media, 2005.

62 S. Belhachi, S. Samah, S. Abdalla, M. W. Iqbal, J. Y. Al-Humaidi, M. G. Batterjee and M. M. Rahman, Comprehensive exploration of rare-earth chalcogenides: A DFT-based investigation into their optoelectronic, elastic, thermomechanical and magnetic properties for advanced functional and high-temperature applications, *Inorg. Chem. Commun.*, 2025, **177**, 114442.

63 L. Wang, Generalized fourier law, *Int. J. Heat Mass Tran.*, 1994, **37**(17), 2627–2634.

64 R. Chegel and S. Behzad, Tunable electronic, optical, and thermal properties of two-dimensional germanene via an external electric field, *Sci. Rep.*, 2020, **10**(1), 704.

65 İ. Yücel, The structural, electronic, optic and thermoelectric properties of impurity doped Mg_2Ge compounds: DFT study, *J. Phys. Chem. Solids*, 2022, **160**, 110351.

66 J. D. Musah, A. M. Ilyas, A. Novitskii, I. Serhiienko, K. O. Egbo, G. Saianand, V. Khovaylo, S. Kwofie, K. M. Yu and V. A. Roy, Effective decoupling of seebeck coefficient and the electrical conductivity through isovalent substitution of erbium in bismuth selenide thermoelectric material, *J. Alloys Compd.*, 2021, **857**, 157559.

67 P. Mavropoulos and I. Galanakis, A review of the electronic and magnetic properties of tetrahedrally bonded half-metallicferromagnets, *J. Phys.: Condens. Matter*, 2007, **19**(31), 315221.